Rift Valley Magmatism – is there Evidence for Laterally Variable Alkali Clinopyroxenite Mantle?

Felicity E. LLOYD[1], Allan R. WOOLLEY[2], Francesco STOPPA[3]**and Nelson G. EBY[4]*

[1] *PRIS, University of Reading, Whiteknights, Reading, RG6 6AB, United Kingdom*
[2] *Department of Mineralogy, Natural History Museum, Cromwell Rd., London SW7 5BD, United Kingdom*
[3] *Department of Geology, Piazza Universita-06123, Perugia, Italy*
[4] *Department of Environmental, Earth and Atmospheric Sciences, University of Massachussetts, Lowell, MA 01854, United States of America*
* *Also at: Department of Geology, Bristol University, Queens Rd., BS8 1RJ, United Kingdom*
** *Also at: Faculty of Siences, Campus Madonna delle Piane, University of G. d'Annunzio, 66013-Chieti Scalo, Italy*

ABSTRACT. Alkali pyroxenite xenoliths from three volcanic fields in Uganda are largely composed of clinopyroxene (cpx) and phlogopite–biotite (together >70% of mode). Inter-field compositional variation in these minerals, shown by 749 cpx analyses and 237 mica analyses from 34 xenoliths, indicates bulk-chemical lateral variation in the xenolith source. The ubiquitous presence of alkali clinopyroxenite xenoliths in all the fields suggests this lithology is widespread beneath Uganda's Western Rift. Nd-Sr and Pb isotope systematics indicate that the xenoliths are not cumulate from their host kamafugites, while P-T experiments indicate that the kamafugites were in equilibrium with clinopyroxenite at ~>60 km depth. It is argued therefore that the xenoliths are fragments of a laterally variable clinopyroxenite layer in Uganda's Western Rift deep crust–mantle.

KEY WORDS: clinopyroxene, phlogopite–biotite, xenolith, lateral heterogeneity, mantle.

Introduction

South West Uganda is noted for effusive carbonatite in the northern Fort Portal field, ultrapotassic (K_2O typically > 3 wt.% and K_2O/Na_2O > 2; Foley et al. 1987) mafic kamafugite diatremes in the central Katwe-Kikorongo and Bunyaruguru fields, and potassic mafic-felsic flows in the southern Bufumbira field (Fig. 1). The central fields are the type area for kamafugites. This classification (Sahama 1974) is based on the diagnostic minerals of the three primary magma types recognised by Holmes (1965) in his classic work on Uganda – katungite (melilite); mafurite (kalsilite) and ugandite (leucite). The unusual activity of the South West Ugandan province is closely tied to the tectonic setting of the uplifted and rifted western edge of the East African Craton.

The K-silicate fields boast abundant alkali clinopyroxenite xenoliths. Elsewhere in the world similar alkali clinopyroxenites are frequently interpreted as cumulate from their host alkaline magmas. In South West Uganda it appears that a cognate origin is precluded by the Nd-Sr and Pb isotope systematics of Katwe-Kikorongo xenoliths, as is also a crustal derivation (Davies and Lloyd 1989). In this study the authors showed that the Katwe-Kikorongo hosts plot near to bulk Earth in terms of $^{87}Sr/^{86}Sr$ (0.7047) and $^{143}Nd/^{144}Nd$ (0.51264) and the xenoliths plot in a closely adjacent field more radiogenic in Sr and less radiogenic in Nd. The Pb isotope systematics discriminate strongly between host lavas and xenoliths. The lavas have limited Pb isotope variation ($^{206}Pb/^{204}Pb$ 19.09–19.19) and are relatively radiogenic ($^{207}Pb/^{204}$ Pb 15.65–15.7 and $^{208}Pb/^{204}Pb$ 39.58–40.03). In contrast the xenoliths vary significantly in Pb isotopes and on Pb/Pb isotope diagrams form linear arrays that extend from slightly less radiogenic than the lavas ($^{206}Pb/^{204}Pb$ 18.95) to values less radiogenic than Group II kimberlites ($^{206}Pb/^{204}Pb$ 17.01). A xenolith Pb isochron was considered unlikely because Nd and Sr isotope systematics are similar for lavas and xenoliths and close to bulk Earth and the authors preferred to postulate a mixing line between end members with a lithospheric and an asthenospheric signature, respectively. It appears that the Nd and Sr isotope results also rule out crustal contamination.

In Uganda, the ubiquitous presence of the xenoliths in the three K-silicate fields, and xenocrysts of similar material in the carbonatites, has led to models that have the potential to generate a widespread layer of clinopyroxenite beneath the West Rift: (1) older alkali clinopyroxenite intrusive complex(es) in the deep crust (Waters 1955); (2) carbonatite melt reacted with granitic crust to produce "crystalline" alkali clinopyroxenite (Holmes 1965); and (3), based on metasomatic + magmatic textures (Holmes 1942; Lloyd and Bailey 1975), lherzolite mantle metasomatised and veined by incompatible- and LIL element-bearing CO_2, H_2O fluids and small volume melts (Lloyd and Bailey 1975; Bailey 1977; Lloyd et al. 1991).

A notable problem is that no lherzolite has been found, only rare dunite and wehrlite showing replacement by phlogopite. There is no geophysical evidence to indicate a clinopyroxenite layer or complexes at shallow levels. The distinct negative gravity anomaly in the West Rift is usually interpreted as a diapir of hot and partially melted lithosphere, but the possibility that it represents a layer of alkali clinopyroxenite (Lloyd and Bailey 1975) cannot be dismissed.

Aim and approach of this investigation

The aim of this project is to compare xenolith minerals to establish whether there is any consistent pattern of regional variation in the xenoliths, as might be expected if they are plucked from a laterally extensive layer at depth.

Collecting strategy was dictated by time and accessibility. Twenty-five xenoliths were collected from four craters in the Katwe-Kikorongo field of which three lie near the borders of the field, namely Kikorongo to the NE (15 xenoliths), Machati in the S-central area (2 xenoliths), and Murumuli to the SE (5 xenoliths). Kasenyi (3 xenoliths) is an isolated cone 12 km E of the main field. Two localities were sampled in Bunyaruguru: Nyungu Crater (2 xenoliths) and Chema Crater (2 xenoliths), and 1 locality in Bufumbira – the Lutale flow (5 xenoliths).

Volc. Field	KATWE-KIKORONGO FIELD									BUNYARUGURU FIELD										BUFUMBIRA FIELD	
Location	Murumuli				Machati		Kikorongo			Kasenyi			Nyungu					Chema		Lutale	
Xenolith	50	50G	50F	50F	65B	65B	78K	78I	78I	85C	85C	85C	103	103	103	103	103	108	108	137D	139
Analysis no.	#72	#65	#3	#21	#117	#121	#5	#39	#4	#35	#37	#38	#14	#19	#20	#29	#30	#3	#17	#36	#6
Comment	Lava ph near rim	Lava ph Edge	In syenite	In syenite	"Clast" rim	"Clast" core	"Clast"	"Clast"	Neoblast	"Clast" inner rim	"Clast" outer rim	"Clast" core	Green interstitial	Al-rich core	Rim to 19	Diopside core	Green rim	"Ciast"	"Clast" rim		
SiO_2	44.05	47.18	52.4	52.89	49.16	50.95	52.43	50.85	51.52	54.43	53.73	52.72	51.93	45.83	52.02	51.76	52.11	46.88	39.85	46.48	50.85
TiO_2	5.18	1.67	0.57	0.18	1.58	1.91	1.28	1.22	1.26	0.54	0.71	1.85	0.54	0.91	0.3	0.29	0.54	1.93	3.76	2.6	0.94
Al_2O_3	5.66	6.48	0.29	0.59	3.54	2.38	1.43	2.65	1.88	0.5	1.55	0.81	0.88	8.1	2.87	2.84	1.09	7.61	13.74	7.85	4.52
FeO^*	6.89	9.71	18.92	28.14	10.13	6.43	4.73	9.55	7.03	5.33	5.57	4.4	13.28	11.49	7.95	8.09	12.7	9.47	9.12	8.34	5.32
Cr_2O_3	0.01	0.07	0.02	0	0.03	0.05	0	0.09	0	0.1	0.14	0.05	0.34	0.36	0.16	0.2	0.37	0.08	0.09	0.2	1.15
MnO	0.15	0.23	0.58	0.23	0.19	0.07	0.05	0.18	0.1	0.15	0.14	0.09	0.27	0.15	0.21	0.18	0.36	0.26	0.09	0.19	0.08
NiO	0.02	0.04	0.05	0	0	0	0.01	0.09	0	0.05	0	0	0.1	0.22	0.01	0.06	0.07	0	0.12	0	0
MgO	12.59	10.9	5.57	0.57	11.35	14.2	15.67	11.95	13.65	15.99	15.26	15.87	9.44	12.54	13.18	13.24	10.05	9.59	8.75	10.63	15.55
CaO	23.88	23.08	15.64	4.8	23.31	24.1	23.54	22.81	23.75	22.48	22.51	24.15	19.88	15.75	23.49	23.38	20.68	22.01	24.35	22.7	21.31
Na_2O	0.48	0.72	4.89	10.54	0.99	0.7	0.74	1.03	0.75	0.9	1.22	0.72	2.93	2.66	0.7	0.75	2.56	1.58	0.12	1.11	0.45
K_2O	0	0.07	0	0.13	0	0	0	0	0	0	0	0	0	0.32	0	0.02	0	0	0	0	0
Total	98.91	100.14	98.93	98.07	100.28	100.79	99.88	100.42	99.94	100.47	100.83	100.66	99.59	98.33	100.89	100.81	100.53	99.41	99.99	100.1	100.17
Mg#	0.767	0.669	0.346	0.035	0.669	0.799	0.856	0.693	0.778	0.844	0.831	0.867	0.448	0.522	0.624	0.621	0.442	0.503	0.49	0.56	0.745
Si#	0.919	0.974	0.992	0.997	0.976	0.973	0.982	0.982	0.982	0.993	0.99	0.974	0.991	0.985	0.996	0.996	0.992	0.97	0.934	0.96	0.986
Si	1.665	1.765	2.013	2.033	1.838	1.869	1.922	1.893	1.91	1.983	1.95	1.921	1.957	1.707	1.913	1.904	1.945	1.762	1.502	1.733	1.863
Aliv	0.252	0.235	0	0	0.156	0.103	0.062	0.107	0.082	0.017	0.05	0.035	0.039	0.293	0.087	0.096	0.048	0.238	0.498	0.267	0.137
Fe^{3+}	0.083	0	0	0	0.006	0.028	0.016	0	0.008	0	0	0.045	0.004	0	0	0	0.007	0	0	0	0
Alvi	0	0.05	0.013	0.027	0	0	0	0.009	0	0.004	0.016	0	0	0.062	0.038	0.027	0	0.099	0.112	0.077	0.058
Ti	0.147	0.047	0.016	0.005	0.044	0.053	0.035	0.034	0.035	0.015	0.019	0.051	0.015	0.025	0.008	0.008	0.015	0.055	0.107	0.073	0.026
Fe^{3+}	0.076	0.144	0.292	0.688	0.144	0.073	0.06	0.101	0.074	0.044	0.076	0.028	0.216	0	0.078	0.1	0.199	0.142	0.177	0.117	0.026
Fe^{2+}	0.059	0.16	0.316	0.217	0.166	0.097	0.069	0.197	0.136	0.118	0.092	0.061	0.199	0.358	0.167	0.148	0.19	0.155	0.11	0.143	0.137
Cr	0	0.002	0.001	0	0.001	0.001	0	0.003	0	0.003	0.004	0.001	0.01	0.011	0.005	0.006	0.011	0.002	0.003	0.006	0.033
Mg	0.709	0.608	0.319	0.033	0.633	0.777	0.856	0.663	0.754	0.868	0.826	0.862	0.53	0.696	0.723	0.726	0.559	0.537	0.492	0.591	0.849
Ni	0.001	0.001	0.002	0	0	0	0	0.003	0	0.001	0	0	0.003	0.007	0	0.002	0.002	0	0.004	0	0
Mn	0.005	0.007	0.019	0.007	0.006	0.002	0.002	0.006	0.003	0.005	0.004	0.003	0.009	0.005	0.007	0.006	0.011	0.008	0.003	0.006	0.002
Ca	0.967	0.925	0.644	0.198	0.934	0.947	0.925	0.91	0.943	0.877	0.875	0.943	0.803	0.629	0.926	0.922	0.827	0.886	0.983	0.907	0.836
Na	0.035	0.052	0.364	0.786	0.072	0.05	0.053	0.074	0.054	0.064	0.086	0.051	0.214	0.192	0.05	0.054	0.185	0.115	0.009	0.08	0.032
K	0	0.003	0	0.006	0	0	0	0	0	0	0	0	0	0.015	0	0	0	0	0	0	0
Sum cations	3.999	3.997	3.999	4	4	4	4	4	3.999	3.999	3.998	4.001	3.999	4	4.002	3.999	3.999	3.999	4	4	3.999
Jadeite	0	2.878	0.798	2.156	0	0	0	0.511	0	0.227	0.87	0	0	3.303	2.011	1.485	0	5.818	0.58	4.501	1.723
Aegirine	2.04	0.299	21.42	61.77	4.003	2.663	2.764	3.546	2.881	3.07	3.698	2.677	12.288	7.666	0.665	1.456	10.518	0.979	0	0.162	0
CaFe Tsch	2.251	8.038	0	0	4.042	1.324	0.364	2.064	1.044	0	0.581	0	0.68	0	3.743	4.275	1.402	7.563	11.27	6.994	3.175
CaTi Tsch	8.314	2.68	0	0	2.462	2.818	1.855	1.852	1.861	0.767	1.031	1.812	0.877	1.349	0.445	0.434	0.861	3.221	6.685	4.238	1.396
CaAl Tsch	0	0	0	0	0	0	0	0	0	0	0	0	0	0	0	0	0	0	6.455	0	1.392
Wollastonite	44.027	42.191	39.16	15.957	45.238	46.51	46.365	45.414	47.065	44.741	44.96	47.352	44.411	31.906	45.44	45.085	44.685	41.534	37.254	41.469	39.127
Enstatite	40.047	34.759	19.405	2.637	35.055	41.525	44.999	35.958	39.961	45.039	43.929	44.953	30.371	36.84	38.744	39.234	31.745	31.717	30.831	34.337	45.781
Ferrosilite	3.321	9.155	19.217	17.481	9.199	5.161	3.652	10.655	7.188	6.155	4.93	3.206	11.373	18.936	8.951	8.032	10.79	9.169	6.925	8.299	7.405
WO	50.923	50.17	40.501	17.304	49.428	49.252	47.968	48.497	49.163	45.871	46.7	48.555	45.603	37.247	48.735	48.447	46.098	51.245	55.702	51.415	45.185
EN	37.356	32.96	20.069	2.859	33.487	40.378	44.428	35.352	39.315	45.398	44.05	44.396	30.13	41.263	38.047	38.173	31.171	31.067	27.85	33.5	45.876
FS	11.721	16.87	39.43	79.837	17.085	10.37	7.604	16.151	11.522	8.731	9.249	7.048	24.267	21.49	13.219	13.38	22.731	17.688	16.447	15.085	8.939
WEF	96.114	94.189	64.042	22.433	92.373	94.819	94.625	92.271	94.455	93.631	91.282	94.838	78.247	81.454	94.804	94.395	81.077	87.33	98.908	91.118	96.616
JD	0	1.506	1.546	2.898	0	0	0	0.661	0	0.581	1.538	0	0	18.546	1.694	1.206	0	5.184	0.424	3.533	2.344
AE	3.886	4.305	34.411	74.668	7.627	5.181	5.375	7.068	5.545	5.788	7.18	5.162	21.753	0	3.502	4.399	18.923	7.486	0.669	5.349	1.04

Table 1. Representative microprobe analyses of clinopyroxenes from Ugandan xenoliths. Analyses are recalculated using "Minpet" version 2.02, according to the scheme of Yoder and Tilley (1962: formula unit normalized to 6 oxygens and recalculated to 4 cations). Fe^{3+} is estimated by charge balance. End-members are recalculated by method of Cawthorn and Collerson (1974) (Tsch = Tschermak's molecule). WO (wollastonite), EN (enstatite), FS (ferrosilite), and WEF (WO+EN+FS), JD(jadeite), AE(aegirine) are IMA end-members for classification in the Ca-Mg-Fe quadrilateral and the jadeite-aegirine-"Quad" diagram. "Machati" is a field name (after our Game Ranger) assigned to an unmapped crater. [ph = phenocryst; Mg# = mol MgO/(MgO+FeO); Si# = mol $SiO_2/(SiO_2+TiO_2)$]

The xenoliths are composed largely of clinopyroxene + phlogopite–biotite (together >70 modal%) with accessory apatite, titanomagnetite, titanite and minor/trace perovskite, calcite and spinel. Variations in clinopyroxene and dark mica compositions account for a large proportion of the variation in xenolith bulk chemistry. Hence, a first approach was microprobe analysis. The xenoliths were probed at the NHM, London, and compositions determined for 489 pyroxenes and 175 micas from the Katwe-Kikorongo xenoliths, and a further 260 pyroxenes and 62 micas were obtained from the xenoliths of Buyaruguru and Bufumbira.

Petrology a geochemistry

Xenolith clinopyroxene and phlogopite compositions

With the exception of two syenite xenoliths, and rare cpx cores from a single xenolith (see below), all clinopyroxenes are diopsides (Di_{95}–Di_{50}), with about 25% plotting above Wo_{50} in the pyroxene quadrilateral (see Table 1). Micas are phlogopite–biotite ranging from Fe/(Fe+Mg) 0.22 to 0.54 and extend to more aluminous compositions (max. 2.986 Al atoms pfu; see 137C #20 Table 2).

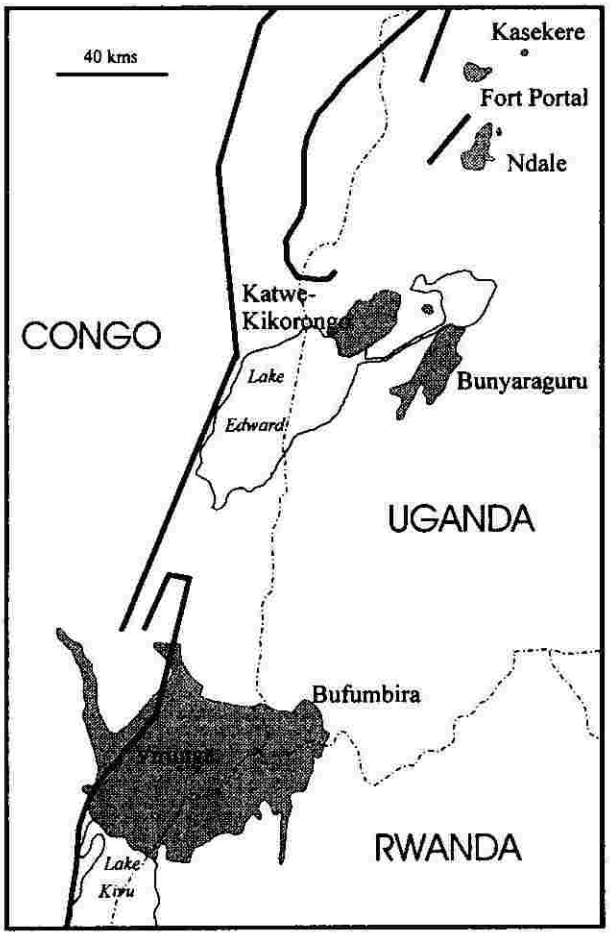

Fig. 1. Map to show the four South West Ugandan volcanic fields in the west branch of the East African Rift system. From north to south: 1 – Fort Portal effusive calcio-carbonatite; 2 and 3 – Central fields of Katwe-Kikorongo and Bunyaruguru ultrapotassic (kamafugites) diatremes; 4 – Southern field of Bufumbira potassic mafic-felsic flows and pyroclasts – part of the larger Virunga field (Uganda–Rwanda–Democratic Republic of Congo). Thick black lines indicate major rift faults.

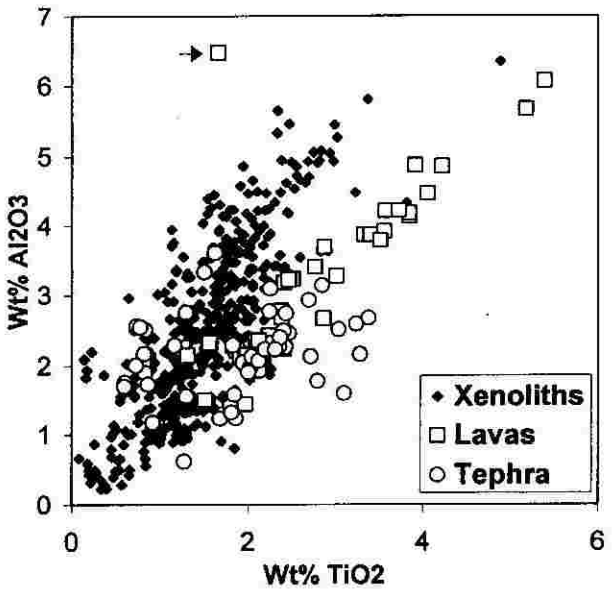

Fig. 2. Clinopyroxenes from Katwe-Kikorongo volcanics plotted in terms of wt.% TiO_2 versus Al_2O_3 (after Mitchell 1985). The "flyer" lava pyroxene is indicated by an arrow.

The Cr contents of both minerals are generally low. Pyroxene Cr_2O_3 ranges from below detection to 1.15 wt.% with the majority of 0.2 wt.% or less (see Table 1). Micas range from below detection to 0.45 wt.% Cr_2O_3 with the majority less than 0.1 wt.% (see Table 2). Detection limit for Cr in both minerals is 0.05% of oxide present. These Cr levels are similar to those of the Cr-poor megacryst suite in South African kimberlites (Gurney et al. 1991, and references therein).

Xenolith micas contain trace to minor Ba, generally between 0.2 and 1 wt.% BaO (see Table 2; detection limit: 0.05% of oxide present), which typically correlates negatively with SiO_2 and positively with Al_2O_3.

Xenoliths and lavas compared

Xenolith and lava clinopyroxenes show distinct trends in terms of TiO_2 versus Al_2O_3 (Fig. 2; compare 50 #72 with other analyses in Table 1). Clinopyroxene crystal lapilli from the tephra are both xenocrysts (fragmented xenolith material) and phenocrysts. The lava clinopyroxenes plotting well within the xenolith field are xenocrystic cores to phenocrysts (such cores have xenolith isotopic signature, see Davies and Lloyd 1989). Xenolith clinopyroxenes plotting on the lava trend petrographically appear likely to be the product of xenolith-host melt interaction. [The "flyer" (arrowed in Fig. 2; 50G #65, Table 1) is from the extreme edge of an oscillation-zoned phenocryst]. The more aluminous xenolith pyroxene probably reflects a higher pressure of crystallisation (see Edgar et al. 1976; Lloyd 1981).

While lava pyroxenes show a clear trend of increasing Ti accompanied by falling Mg# [(mol MgO/(MgO+FeO)] and Si# (mol $SiO_2/(SiO_2+TiO_2)$, xenolith pyroxene describes a broader field (Fig. 3) that overlaps the more magnesian lava pyroxene and extends to higher Si# – adjacent to pyroxenes from kimberlite and MARID. The xenolith field also extends to more iron-rich (lower Mg#) clinopyroxenes. The isolated low-Ti, high-Fe samples (indicated by arrows) are aegirine-augite–aegirine from

Volc. Field	KATWE-KIKORONGO																BUNYARUGURU			BUFUMBIRA			
Location	Nnab	Kabafu	Nab L	Nab L	Katwe	Murumuli			Machati		Kikorongo						Kasenyi	Nyungu		Lutale			
Xenolith						50A	50E	50D	65A	65B	78E	78F	78I	78K	78K	78N	85C	103	103	104	137C	137D	139
Lava	K4.5	K11B	K6.4	K6.4	K17.1																		
Analysis no.	#11	#1	#1	#17	#1	#6	#37	#101	#78	#65	#38	#12	#57	#19	#58	#8	#48	#18	#7	#1	#20	#49	#10
Comment	Gr'mass	Gr'mass	Pheno-cryst	Gr'mass	Mega-cryst	Poikilitic		Encloses cpx			Core zone			In cpx clast	Large plate		Large plate	Inter-stitial	Inter-stitial				
SiO_2	44.43	40.64	38.11	34.88	37.08	35.9	36.86	37.12	37.25	36.11	40.37	35.09	37.33	38.81	37.7	36.53	38.53	40.03	36.97	36.38	35.99	35.4	37.38
TiO_2	1.4	6.04	8.08	8.07	6.58	3.17	2.54	4.42	3.08	5.41	1.59	6.74	5.81	4.43	4.54	8.25	6.92	4.1	5.71	6.53	7.39	7.47	5.97
Al_2O_3	7.37	8.01	11.09	13.66	14.19	14.27	14.08	15.14	15.4	14.14	11.55	13.94	13.74	14.72	12.72	14.14	12.77	11.34	10.53	12.78	17.44	15.12	15.22
Cr_2O_3	0.05	0.01	0	0	0.43	0	0.11	0.09	0.07	0	0	0.09	0	0	0.04	0.08	0.2	0.1	0.13	0	0.24	0.09	0.45
FeO	6.63	8.5	12.87	8.48	8.99	20.28	17.23	10.24	9.74	15.83	10.29	11.1	13.53	8.23	11.51	11.49	9.24	13.87	13.6	18.76	9.67	14.15	9.38
MnO	0.05	0.11	0.08	0.13	0.02	0.32	0.17	0.17	0.15	0.25	0.1	0.08	0.07	0.07	0.11	0.08	0.1	0.19	0.12	0.18	0.05	0.13	0.05
MgO	22.78	19.39	15.12	17.18	18.1	11.76	13.51	18.04	19.8	14.24	21	14.61	16.1	19.98	17.77	15.35	18.41	13.55	15.28	11.81	15.38	12.78	16.78
CaO	0.38	0.07	0.14	0.01	0	0	0	0.06	0.06	0.06	0	0.21	0.1	0.12	0	0.26	0.05	0.55	0.02	0.01	0.15	0.02	0.08
BaO	0.48	0.06	1.8	6.9	0.37	0.48	0.21	0.86	0.55	0.55	0.11	0.55	0.38	0.2	0.28	0.52	0.28	0.15	0.13	0.28	0	0	0
Na_2O	1.24	0.75	0.48	0.66	0.26	0.28	0.44	0.32	0.25	0.29	0.28	0.34	0.28	0.75	0.38	0.23	0.32	1.12	0.24	0.26	0.89	0.5	0.78
K_2O	9.84	10.41	8.98	7.06	9.62	9.32	9.5	9.23	9.63	9.73	10.13	9.21	9.85	9.19	9.72	9.53	10.05	9.99	9.86	9.81	7.84	8.34	8.65
F	6.72	2.09	3.5	3.61	0.14	0	0.42	0.46	0.01	0	0.02	0	0	0	0	0	0	0	0	0	0.47	0.47	0.46
Total	101.37	96.08	100.25	100.64	95.78	96.05	95.07	96.15	95.99	96.61	95.44	91.96	97.19	96.5	94.77	96.46	96.87	94.99	92.59	96.8	95.51	94.47	95.2
O_F	2.83	0.88	1.47	1.52	0.06	0.11	0.18	0.19	0	0	0.01	0	0	0	0	0	0	0	0	0	0.2	0.2	0.19
Total (a)	98.54	95.2	98.78	99.12	95.72	95.94	94.89	95.96	95.99	96.61	95.43	91.96	97.19	96.5	94.77	96.46	96.87	94.99	92.59	96.8	95.31	94.27	95.01
Mg#	0.86	0.803	0.677	0.783	0.782	0.508	0.583	0.759	0.784	0.616	0.785	0.701	0.68	0.812	0.734	0.704	0.78	0.635	0.667	0.529	0.739	0.617	0.761
Si#	0.977	0.9	0.863	0.852	0.883	0.937	0.951	0.918	0.942	0.899	0.971	0.874	0.895	0.921	0.917	0.855	0.884	0.929	0.896	0.881	0.867	0.863	0.893
											Number of ions on the basis of 22 oxygens												
Si	6.444	6.036	5.65	5.23	5.413	5.524	5.638	5.445	5.431	5.411	5.908	5.404	5.479	5.55	5.617	5.361	5.561	6.013	5.722	5.51	5.233	5.345	5.466
Ti	0.153	0.675	0.901	0.91	0.722	0.367	0.292	0.488	0.338	0.61	0.175	0.781	0.641	0.477	0.509	0.911	0.751	0.463	0.665	0.744	0.808	0.848	0.657
Al	1.259	1.401	1.936	2.412	2.439	2.586	2.536	2.616	2.644	2.495	1.991	2.528	2.375	2.479	2.232	2.444	2.171	2.006	1.919	2.279	2.986	2.689	2.621
Fe^*	0.804	1.056	1.596	1.063	1.097	2.61	2.204	1.256	1.188	1.984	1.259	1.43	1.661	0.984	1.434	1.41	1.115	1.742	1.76	2.376	1.176	1.787	1.147
Cr	0.006	0.001	0	0	0.05	0	0.013	0.01	0.008	0	0	0.011	0	0	0.005	0.009	0.023	0.012	0.016	0	0.028	0.011	0.052
Mn	0.006	0.014	0.01	0.017	0.002	0.042	0.022	0.021	0.019	0.032	0.012	0.01	0.009	0.008	0.014	0.01	0.012	0.024	0.016	0.023	0.006	0.017	0.006
Mg	4.926	4.293	3.341	3.84	3.939	2.698	3.081	3.945	4.303	3.181	4.582	3.354	3.523	4.26	3.947	3.358	3.961	3.034	3.525	2.666	3.334	2.877	3.658
Ca	0.059	0.011	0.022	0.002	0	0	0	0.009	0.009	0.01	0	0.035	0.016	0.018	0	0.041	0.008	0.089	0.003	0.002	0.023	0.003	0.013
Ba	0.027	0.003	0.105	0.405	0.021	0.029	0.013	0.049	0.031	0.032	0.006	0.033	0.022	0.011	0.016	0.03	0.016	0.009	0.008	0.017	0	0	0
Na	0.349	0.216	0.138	0.192	0.074	0.084	0.13	0.091	0.071	0.084	0.079	0.102	0.08	0.208	0.11	0.065	0.09	0.326	0.072	0.076	0.251	0.146	0.221
K	1.821	1.973	1.698	1.35	1.791	1.83	1.854	1.727	1.791	1.86	1.891	1.81	1.844	1.677	1.848	1.784	1.85	1.914	1.947	1.895	1.454	1.607	1.614
Sum cations	15.854	15.679	15.397	15.421	15.548	15.77	15.783	15.657	15.833	15.699	15.903	15.498	15.65	15.672	15.732	15.423	15.558	15.632	15.653	15.588	15.299	15.33	15.455
F cations	6.165	1.963	3.282	3.423	0.129	0	0.406	0.427	0.009	0	0.019	0	0	0	0	0	0	0	0	0	0.432	0.449	0.425

Table 2. Representative microprobe analyses of micas from Ugandan xenoliths. Abbreviations: Nnab – crater to N of Nabugando; Nab L – Nabugando lava flow; Gr'mass – groundmass; cpx – clinopyroxene; Mg# – mol MgO/(MgO+FeO); Si# – mol $SiO_2/(SiO_2+TiO_2)$

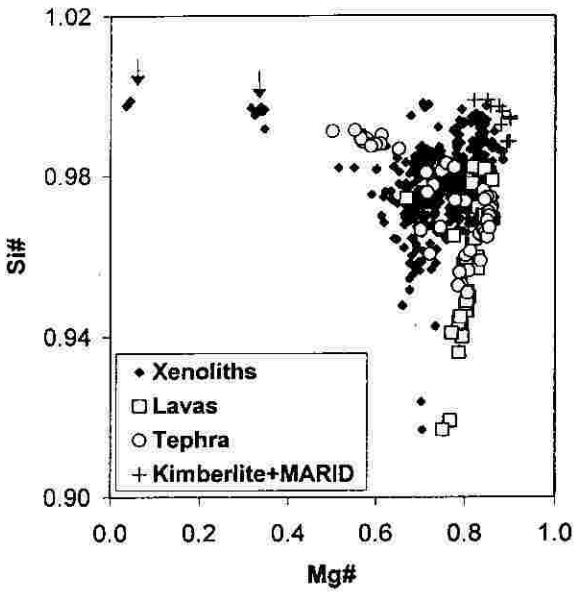

Fig. 3. Clinopyroxene from Katwe-Kikorongo volcanics plotted in terms of mol MgO/(MgO+FeO) (Mg#) versus mol $SiO_2/(SiO_2+TiO_2)$ (Si#) (adapted from Rock 1991). The isolated low-Ti, high-Fe samples are aegirine-augite and aegirine from two syenite xenoliths (arrowed).

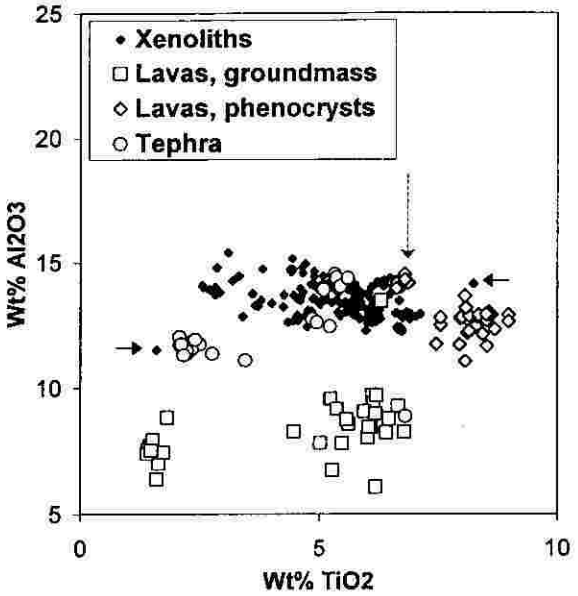

Fig. 4. Micas from Katwe-Kikorongo volcanics in terms of wt.% TiO_2 versus Al_2O_3. The phenocrysts that plot with the xenoliths (sample K17,1 dashed vertical arrow) are large embayed plates and might be better termed megacrysts since their origin as phenocrysts/megacrysts is ambiguous. The reason for the lava micas plotting in two separate groups is given in the text; the two xenolith micas that plot anomalously are indicated by short horizontal arrows. Lava micas, unpublished data, A.D. Edgar and F.E. Lloyd.

one of two rare syenite xenoliths (50F #s 3, 21 Table 1). Tephra pyroxenes again plot as two populations. The anomalous cases are the same as those described for the previous plot.

The broad composition field formed by xenolith cpx appears to imply variable conditions of crystallisation, which is supported by evidence of poly-episodic, disequilibrium mineralogy in individual xenoliths (see Xenolith heterogeneity).

Xenolith mica is more aluminous than the late-crystallising mica in the lavas (Table 2, compare K4,5 #11, K11B #1 with the others) and lava phenocryst mica is more titaniferous (Fig. 4; Table 2, K6,4 #1). Mica crystal lapilli in the tephra are of both xenolith and lava provenance. In Fig. 4 the lava groundmass micas plot in two groups which reflect different residual liquids: (1) a left-hand group of olivine melilitites (katungites; Table 2, K4,5 #11); and (2) a right-hand group of nepheline leucitites (Table 2, K11B #1). There is no immediate explanation for the two xenolith micas that plot anomalously (indicated by broad arrow; left in Fig. 4 = 78E #38 and right = 78N #8, see Table 2). In terms of Mg# and Si# (Fig. 5) the lava micas, although in separate groupings for the reasons described for Fig. 4, show a distinct trend that is similar to that of the lava pyroxene, i.e. of decreasing Mg# with increasing Ti (also Al, see Fig 4). The phenocrysts plot at the Ti-rich end of this trend while late-crystallising micas are richer in Mg- and Si. Xenolith micas cover a broad composition field showing that like the coexisting pyroxene they were also subject to variable conditions of crystallisation.

The chrome content of pyroxenes and micas does not discriminate xenolith and lava parageneses. In the lavas both minerals mostly contain less than 0.2 wt.%, but so do a significant proportion of the xenolith pyroxenes and micas. A few lava phenocrysts (xenocrysts ?) show levels comparable to the higher values seen in the xenolith minerals (Table 2, K17 #1).

Barium levels in some lava micas are the same as for the xenoliths, but they can reach >6 wt.% BaO in the microphenocrysts and interstitial groundmass flakes of particular flows or ejected blocks (e.g. K6,4 #17,Table 2). Such high levels have never been observed in the xenolith micas. High Ba has been reported for micas in other kamafugite lavas (cf. Edgar and Vukadinovic 1992) and such micas are probably a product of late-stage Ba enrichment in some kamafugite residual liquids.

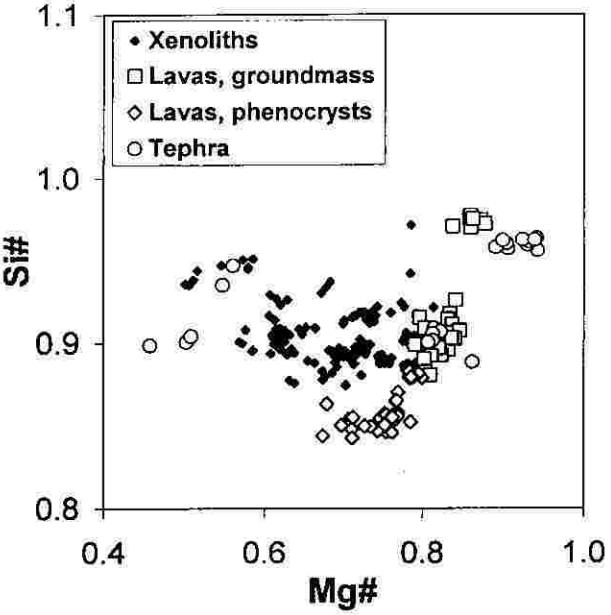

Fig. 5. Micas from Katwe-Kikorongo volcanics in terms of Mg# versus Si#.

Xenolith inter-crater and within-crater variation in the Katwe-Kikorongo field

In terms of Al_2O_3 versus TiO_2 and Mg# versus Si#, the large populations of Kikorongo pyroxene and mica compositions only partially overlap the composition fields described by the smaller populations of pyroxene and mica from the other three craters. Variation between xenoliths from the same crater and variation within single xenoliths (mineral zoning, two generations of pyroxene/mica) is also evident. These features will be described and illustrated more fully elsewhere (F.E. Lloyd, A.R. Woolley, N. Eby and F. Stoppa in prep.).

Inter-field variation

When the Katwe-Kikorongo xenolith pyroxene and mica are compared with those from adjacent fields, the overlap between the large population of Katwe-Kikorongo samples and the adjacent smaller populations is marginal. This seems to indicate strongly that clinopyroxene and dark mica from the other fields extend to compositions not found in Katwe-Kikorongo and that the variation is real and not an artefact of sampling limitations. Clinopyroxene (Fig. 6) from Bunyaruguru overlaps the lower TiO_2- and Al_2O_3-pyroxene of neighbouring Katwe-Kikorongo but extends to compositions with higher Al_2O_3 at this low level of TiO_2, which reflect a small jadeite component as well as increased Al^{vi} (ca. 2–5% Jd; Table 1, 103 #s 19, 20; 108 #3).

Rare cores to Bunyaruguru diopside from a single xenolith (see Fig. 6 and Table 1, 103 #19) and a Tschermak's-rich rim (see Fig. 6 and Table 1, 108 #17) show exceptionally high Al_2O_3 contents (see Xenolith heterogeneity). Bufumbira clinopyroxenes continue the main Bunyaruguru trend to higher-Al values (e.g. 137D #36, Table 1). Fort Portal xenocryst pyroxene (Barker and Nixon 1989) plots with the Katwe-Kikorongo xenoliths. There is poor discrimination between the fields for pyroxene in terms of Mg# versus Si#, as even from a single xenolith pyroxene can show a large range in Mg# (see Xenolith heterogeneity).

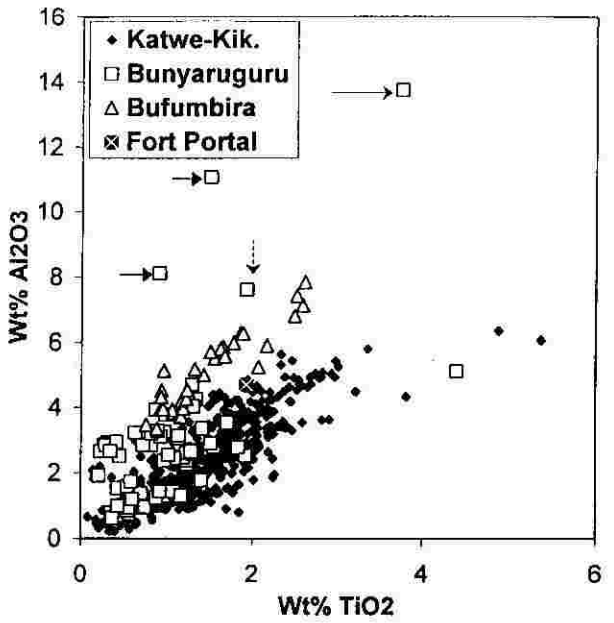

Fig. 6. Clinopyroxenes from Katwe-Kikorongo xenoliths and xenolith clinopyroxenes from adjacent fields on plot of wt.% TiO_2 versus Al_2O_3. Omphacitic cores to Bunyaruguru diopside (sample #103) are arrowed; other anomalous Bunyaruguru pyroxene all from #108: Jd-bearing "clast" indicated by dashed vertical arrow; CaFe+CaAl+CaTi-Tschermak's rich rim to a "clast" indicated by dotted arrow; high-Ti granule enclosed in perovskite, plotting with Katwe-Kikorongo samples.

Phlogopite–biotite (Fig. 7) shows a similar TiO_2 range for all three fields extending to lower values for Katwe-Kikorongo (e.g. 50E #37, Table 2; the lowest TiO_2 – 78E #38 – is anomalous, see Fig. 4). Alumina varies more significantly: Bunyaruguru mica overlaps with Katwe-Kikorongo but extends to lower Al_2O_3 values (103 #7, Table 2); Bufumbira mica follows its coexisting pyroxene with the highest Al_2O_3 values (Table 2) suggesting that higher-Al is a bulk-composition signature for these Bufumbira xenoliths. Dark micas discriminate quite well between the fields in terms of Mg# versus Si# (Fig. 8). Katwe-Kikorongo micas have the greatest Mg# range (50A #6-78K #19, Table 2) and cover a higher range of Si# values (78F#12-50E #37, the highest Si# is anomalous 78E #38 in Fig. 4) only slightly overlapping Bunyaruguru and Bufumbira. The high Al in the micas of Bufumbira is reflected in their low Si contents (137D # 49, 137C #20, Table 2), while micas of Bunyaruguru have lower Mg# (lowest = 104 #1, Table 2) than those of Bufumbira but generally higher Si# and occupy a separate field between Katwe-Kikorongo and Bufumbira (e.g. compare 103 #18 with 137D #49, Table 2). Higher Cr, in addition to higher Al, also appears to be significant in Bufumbira clinopyroxenes and micas which range to the highest values of Cr seen in the Ugandan fields (see, 139 #6, Table 1 and 139 #10, Table 2, respectively).

Xenolith heterogeneity and complex crystallisation history

This study has revealed complex and different crystallisation histories for many of the xenoliths. For example later-crystallising pyroxene granules often have higher Mg# (e.g. sample 78I #4, Table 1: avg Mg# 0.77) than the earlier coarse "clastic" looking pyroxenes (78I #39, Table 1: avg Mg# 0.70) they surround. Small mica flakes, in sub-ophitic to interstitial relationship with the granules, typically have lower Mg# (e.g. 78I #57, Table 2: avg. Mg# 0.69) similar to the early, coarse pyroxene.

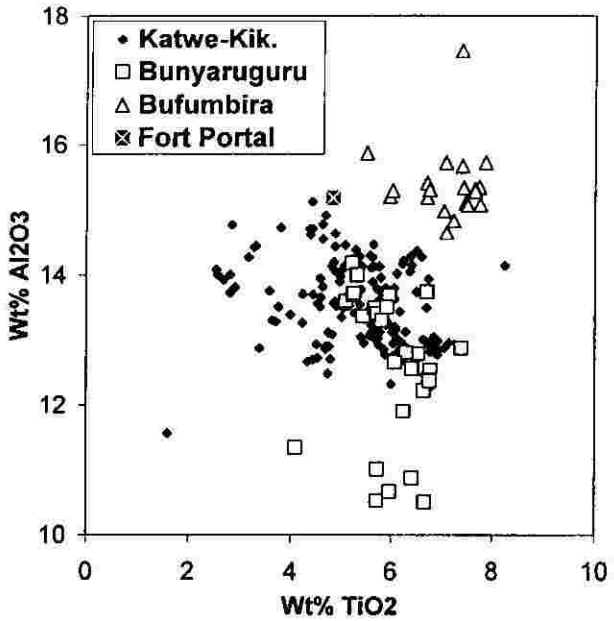

Fig. 7. Micas from Katwe-Kikorongo xenoliths and xenolith micas from adjacent fields on plot of Al_2O_3 versus TiO_2.

This may indicate that the minerals are in disequilibrium, as analyses of co-crystallising liquidus clinopyroxene and mica of melting experiments on Ugandan lava and xenolith compositions (Edgar et al. 1976; Lloyd et al. 1986) show similar Mg#. Zoning in clinopyroxenes can be oscillatory but in other cases resembles overgrowth of earlier more- or less-iron-rich diopside by later less- or more-iron-rich diopside.

A xenolith from Nyungu Crater, Bunyaruguru (#103) contains dispersed "clasts" of highly strained colourless diopside (e.g. 103 #29, Table 1) that are rimmed by unstrained green iron-rich pyroxene and surrounded by iron-rich pyroxene granules (e.g. 103 #s 30, 14, Table 1) and biotite flakes (103 #s 7, 18, Table 2). Rarely, the colourless clasts contain anhedral very pale greeny brown cores of an earlier Si-poor, Al- and Na-rich (?) pyroxene, with trace Ni as well as Cr (103, #19, Table 1). The analyses have low totals and a small degree of alteration cannot be ruled out; trace K may indicate slight contamination from mica flakes that are found along the strain lamellae. This means that the end-member calculations will be compromised (see Table 1 for conflicting results of IMA and Cawthorn and Collerson). More of these cores need to be found and analysed before positive identification is made. In another Bunyaruguru sample (#108) occasional rounded isolated cpx is jadeite-bearing diopside (108 #3, Table 1) and heterogeneity is shown by other pyroxenes in this sample (see Fig. 6 and caption, also Table 1).

Lateral heterogeneity in xenolith carbonates and a carbonatite connection

The four Katwe-Kikorongo craters sampled contain some xenoliths with carbonate which varies from calcite to Mg-calcite to dolomite. The vast majority have SrO contents > 0.5 wt.% suggesting a primary igneous origin. Where SrO levels are lower, reaction with meteoric water and recrystallisation has probably occurred. The carbonates show some inter-crater variations (Fig. 9): Murumuli clinopyroxenite carbonates are Mg-calcites, like those of Kikorongo, but one Mg-calcite grain was found adjacent to dolomite with a small Mg-excess over stoichiometric (23.9 wt.% MgO; tie-line in Fig. 9). A Kikorongo Mg-calcite has the highest SrO content recorded (2.7 wt.%). Machati carbonates are nearly pure calcite (zero MnO and trace FeO) with generally lower SrO contents than the carbonates of the other craters; nearly pure calcite from Murumuli syenites has significantly higher SrO. The single carbonate found from Kasenyi is dolomite.

The fact that only one xenolith from Bunyaruguru contained carbonate (Sr-calcite) and that no carbonate has been found in Bufumbira could be a consequence of the considerably smaller xenolith populations investigated from these fields. Interestingly, previous petrological studies of a different xenolith collection produced a similar result (Table 5 of Lloyd et al. 1991) and thus could reflect a greater presence of carbonatite in the Katwe-Kikorongo field. Such a suggestion appears to be endorsed by the recent discovery of a Sr-dolomite carbonatite bomb (F. Stoppa, A.R.Woolley, N. Eby and F.E. Lloyd, in preparation) in the olivine melilitite tuffs of Murumuli Crater. This is incontrovertible evidence of the activity, in the Katwe-Kikorongo field, of a separate, high-temperature carbonatite melt, intimately associated with K-rich olivine melilitite (katungite), which also appears to be reflected in the xenolith mineralogy of this field.

Implications for the deep crust–mantle beneath Uganda

There is no geobarometer for the clinopyroxenites. Pressure–temperature liquidus experiments on Holmes' three primary magmas can suggest possible depths of clinopyroxenite derivation. Melting experiments on katungite (olivine melilitite), with 5% H_2O added, showed olivine as the liquidus phase up to 20 kbar. Above this pressure clinopyroxene replaced olivine on the liquidus (ca. 1,200°C) and phlogopite separated at 80–100°

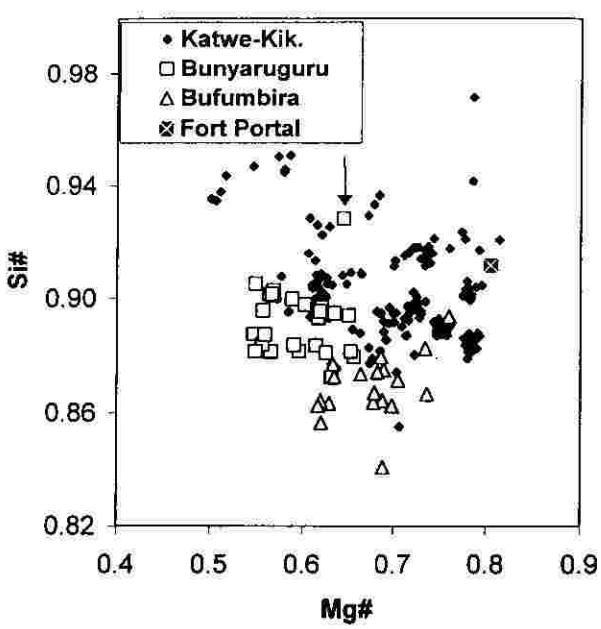

Fig. 8. Micas from Katwe-Kikorongo xenoliths and xenolith micas from adjacent fields on plot of Mg# versus Si#. The single Bunyaruguru analysis with high Si (arrowed) is from #103 in which the omphacite cores are found.

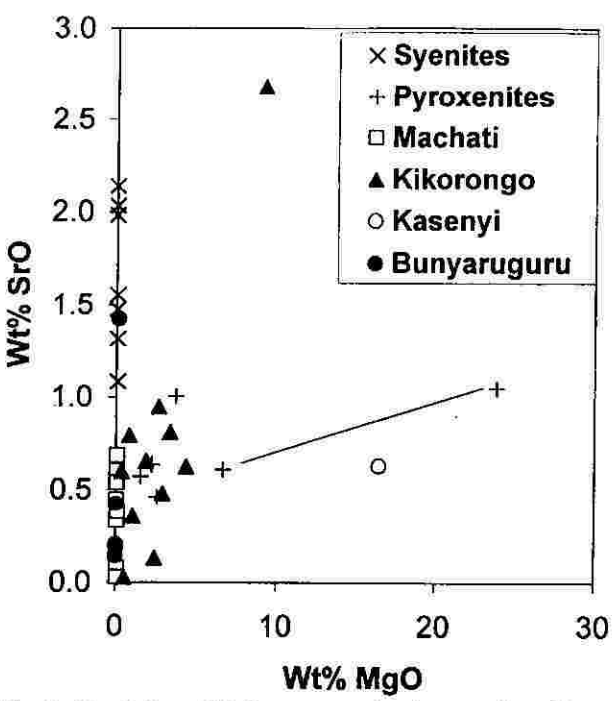

Fig. 9. The SrO and MgO contents of carbonates from Ugandan xenoliths, most of which are from the four Katwe-Kikorongo craters. Tie-line joins adjacent grains of Mg-calcite and dolomite in #50C, Murumuli crater. "Syenites" and "pyroxenites" are from Murumuli Crater. Samples from the other three craters are all pyroxenites.

below this, suggesting the reaction olivine+liquid = phlogopite+liquid (Arima and Edgar 1983). Likewise olivine was absent and clinopyroxene was the liquidus phase above 20 kbar with added $H_2O + CO_2$ ($X_{CO2} = 0.75$). Similar experiments on biotite mafurite (phlogopite–biotite+kalsilite+clinopyroxene) showed a diminishing olivine field with pressure and at 1,250°C and 30 kbar clinopyroxene and phlogopite were the liquidus minerals and there appeared to be a reaction relation between olivine and liquid (Edgar et al. 1976). From these experiments it appears that the kamafugite hosts to the xenoliths are in equilibrium with clinopyroxenite at depths of ca. 60–90 km.

Although this investigation focuses on lateral variation, it is striking that clinopyroxenite appears to be widespread, and its main mineralogy is essentially the same. This would seem to necessitate a horizon of alkali clinopyroxenite in the Ugandan mantle beneath Katwe-Kikorongo and Bunyaruguru and extending north to Fort Portal to provide the xenocryst suite in these rocks (Barker and Nixon 1989).

In the Bufumbira field olivine-rich xenoliths are more common (Holmes and Harwood 1937; Barafaijo 1995). Pressure–temperature experiments by Edgar et al. (1980) on type ugandite (leucite melabasanite) from this field, with 5% H_2O added, showed olivine persisting up to 30 kbar where it was joined by clinopyroxene only 20°C below the liquidus, suggesting that clinopyroxene may become the liquidus phase at P slightly >30 kbar. With H_2O and CO_2 added ($X_{CO2} = 0.75$) clinopyroxene, orthopyroxene, and olivine are near-liquidus phases at 20 kbar but at 30 kbar olivine is absent and garnet joins clinopyroxene and orthopyroxene. Edgar et al. (1980) concluded that ugandite could have a K-enriched (phlogopite is assumed to be a subsolidus phase) wehrlite or lherzolite source at ca. 90 km. In which case it is possible that the clinopyroxenite layer becomes more diffuse southward.

Such an alkali clinopyroxenite layer would equate with the stockwork of metasomatised mantle proposed to exist beneath rifted continental regions dominated by alkaline magmatism (Lloyd and Bailey 1975; Bailey 1982). Mantle alteration is considered to occur by upward percolation of K-rich and incompatible- and RE-element-bearing media (supercritical fluids and small-degree melts) together with carbonate melts towards major weaknesses in crustal lithosphere (Bailey 1977). Mineral separates (cpx, apatite) from Katwe-Kikorongo xenoliths show LREE enrichment and MREE depletion (Davies and Lloyd 1989) which might indicate that source fluids/melts were in equilibrium with mantle garnet.

References

ARIMA M. and EDGAR A.D. 1983. High pressure experimental studies on a katungite and their bearing on the genesis of some potassium-rich magmas of the west branch of the African Rift. *J. Petrol.*, 24, 166–187.

BAILEY D.K. 1977. Lithosphere control of continental rift magmatism. *J. Geol. Soc. London*, 133, 103–106.

BAILEY D.K. 1982. Mantle metasomatism – continuing chemical change within the Earth. *Nature*, 296, 525–530.

BARAFAIJO E. 1995. Mantle metasomatism beneath the Bufumbira volcanic field, SW Uganda. *Berl. Geowiss. Abh.*, A175, 37–45.

BARKER D.S. and NIXON P.H. 1989. High-Ca, low-alkali carbonatite volcanism at Fort Portal, Uganda. *Contrib. Mineral. Petrol.*, 103, 166–177.

DAVIES G.R. and LLOYD F.E. 1989. Pb-Sr-Nd isotope and trace element data bearing on the origin of the potassic subcontinental lithosphere beneath south-west Uganda. *Proceedings of the 4th International Kimberlite Conference, Volume 2*, 784–794. Perth, Western Australia, 1986.

EDGAR A.D. 1991. Source regions for ultrapotassic mafic-ultramafic magmatism in the southwest Uganda region of the African Rift: implications from experimental studies. In KAMPUNZU A.B. and LUBALA R.T. (eds.): *Magmatism in extensional structural settings: the Phanerozoic African Plate*, 73–84. *Springer-Verlag*, Berlin, Heidelberg, New York.

EDGAR A.D., CONDLIFFE E., BARNETT R.L. and SHIRRAN R.J. 1980. An experimental study of an olivine ugandite magma and mechanisms for the formation of its K-enriched derivatives. *J. Petrol.*, 21, 475–497.

EDGAR A.D., GREEN D.H. and HIBBERSON W.O. 1976. Experimental petrology of a highly potassic magma. *J. Petrol.*, 17, 339–356.

EDGAR A.D. and VUKADINOVIC D. 1992. Implications of experimental petrology to the evolution of ultrapotassic rocks. *Lithos*, 28, 188–206.

FOLEY S.F., VENTURELLI G., GREEN D.H. and TOSCANI L. 1987. The ultrapotassic rocks, characteristics, classification and constraints for petrogenetic models. *Earth Science Reviews*, 24, 81–134.

GURNEY J.J., MOORE R.O., OTTER M.L., KIRKLEY M.B., HOPS J.J. and McCANDLESS T.E. 1991. Southern African kimberlites and their xenoliths. In KAMPUNZU A.B. and LUBALA R.T. (eds.): *Magmatism in extensional structural settings, the Phanerozoic African Plate*, 495–536. *Springer-Verlag*, Berlin, Heidelberg, New York.

HOLMES A. 1942. A suite of volcanic rocks from South West Uganda containing kalsilite (a polymorph of $KAlSiO_4$). *Mineral. Mag.*, 26, 197–217.

HOLMES A., 1965. *Principles of physical geology, 2nd. Edition*. Nelson, 1288 pp. London.

HOLMES A. and HARWOOD H.F. 1937. The petrology of the volcanic area of Bufumbira, south-west Uganda. *Memoir of the Geological Survey of Uganda*, 3, 1–300.

LLOYD F.E. 1981. Upper mantle metasomatism beneath a continental rift, clinopyroxenes in alkali mafic lavas and nodules from South-West Uganda. *Mineral. Mag.*, 44, 315–323.

LLOYD F.E., ARIMA M. and EDGAR A.D. 1986. Partial melting of a metasomatised mantle assemblage; an experimental study bearing on the origin of highly potassic continental rift volcanics. *Contrib. Mineral. Petrol.*, 91, 321–329.

LLOYD F.E. and BAILEY D.K. 1975. Light element metasomatism of the continental mantle, the evidence and the consequences. *Phys. Chem. Earth*, 9, 389–416.

LLOYD F.E., HUNTINGDON A.T., DAVIES G.R. and NIXON P.H. 1991. Phanerozoic volcanism of Southwest Uganda, a case for regional K and LILE enrichment of the lithosphere beneath a domed and rifted continental plate. In KAMPUNZU A.B. and LUBALA R.T. (eds.): *Magmatism in extensional structural settings, the Phanerozoic African Plate*, 23–72. *Springer-Verlag*, Berlin, Heidelberg, New York.

MITCHELL R.H., 1985. A review of the mineralogy of lamproites. *Trans. Geol. Soc. S. Afr.*, 88, 411–437.

ROCK N.M.S., 1991. *Lamprophyres*. Blackie and Son Ltd., 285 pp. Glasgow, London.

WATERS A.C. 1955. Volcanic rocks and the tectonic style. *Geol. Soc. Am. Spec. Paper*, 62, 703–722.